RSC Mechanochemistry

ROYAL SOCIETY OF CHEMISTRY

PAPER

View Article Online
View Journal

Check for updates

Cite this: DOI: 10.1039/d5mr00101c

Upgrading coal tar products into hypercrosslinked polymers by mechanosynthesis

A. M. Borrero-López, [ab] J. Castro-Gutiérrez, [*a] E. Derveaux, [cd] W. Marchal, [cd] A. Celzard [ae] and V. Fierro [*a]

Received 13th August 2025
Accepted 23rd April 2026

DOI: 10.1039/d5mr00101c

rsc.li/RSCMechanochem

This study explores the viability of mechanosynthesis (MS) as an environmentally friendly approach for producing hypercrosslinked polymers (HCPs) from various coal tar products (CTPs): creosote, phenolic oil, naphthalene oil, and depleted naphthalene oil (DNO). Thus, aiming to convert dangerous industrial byproducts into high-value materials. Benzene was used as a model molecule, for which a 20–30-minutes reaction time proved optimal for benzene-derived HCPs with high surface area. HCPs produced from CTPs by mechanosynthesis were highly dependent on precursor and reaction conditions. The two most promising CTPs, namely those derived from creosote and DNO, were synthesized with a low catalyst and/or crosslinker content, contrary to literature findings. Creosote- and DNO-derived HCPs with the highest surface areas, ~500 m^2 g^{-1}, were tested as methylene blue (MB) adsorbents and showed a maximum adsorption capacity of 10.2 g_{MB} per 100 g sample, similar to that achieved by other HCPs with higher surface areas.

1 Introduction

The possibility of obtaining stable rigid structures with entangled conformations, and therefore porous materials with high surface areas and pore volumes in the nano/mesoporous ranges, has fostered the application of hypercrosslinked polymers (HCPs) in many different fields, such as drug delivery,[1] catalysis,[2,3] dye removal,[4] heavy metal elimination,[5] chromatography,[6] among others. The formulation of these HCPs is frequently based on solvent-based Friedel–Crafts (FC) and Scholl coupling (SC) reactions, where liquid media such as dichloroethane and precursors such as carbazole, benzene, styrene, divinylbenzene, triphenylbenzene, among others, are frequently used.[7,8] In this context, some research groups are focusing their efforts on developing more environmentally friendly strategies for producing these HCPs, without resorting to hazardous solvents, using bio-based precursors or by-products, and/or significantly reducing the high temperatures and reaction times frequently used, and therefore the energy required to produce the entangled networks.[9–12]

Mechanosynthesis (MS), an old but increasingly attractive process, is one of the most interesting technologies capable of improving eco-friendly and energy-saving approaches over current mainstream approaches. This is due to the interesting properties that can be brought to the formulations developed, as well as to the significant reduction in energy consumed by conventional room-temperature reactions and rapid protocols.[13] MS reactions can be carried out without the presence of a homogenizing media, providing suitable products by mixing solid–solid or liquid–solid reagents, without the need for solvents.[11] Furthermore, MS also enables the properties of the HCPs developed to be adjusted by varying the reaction time, the catalyst/precursor/monomer ratio, the bowl and ball materials or the number of balls, among others.[9,10]

On the one hand, the use of pure, expensive precursors for the production of HCPs can be avoided by using low-cost industrial by-products, as shown by Liu *et al.*,[12] who used HCPs derived from lignin to remove iodine. On the other hand, aromatic compounds, which form the main backbone of conventional HCPs, are widely present in the by-products and residues of petrochemical industries. As far as we know, two studies have demonstrated the use of petrochemical by-products as HCP precursors. Pei *et al.*[11] prepared a HCP based on chloromethylated pitch, which was used as a catalyst for biodiesel synthesis. Gao *et al.*[14] also synthetized pitch-derived HCPs and used them for gas adsorption. Indeed, the industrial production of pitch and naphthalene, for example, entails the production of various low-value by-products, such as chrysene oil, wash oil, distillates, creosote, naphthalene oil and depleted naphthalene oil. These by-products contain large

[a]Université de Lorraine, CNRS, Institut Jean Lamour (IJL), F-88000 Epinal, France. E-mail: jimena.castro-gutierrez@univ-lorraine.fr; vanessa.fierro@univ-lorraine.fr
[b]Pro2TecS – Chemical Process and Product Technology Research Centre, Department Chemical Engineering, ETSI, Universidad de Huelva, Campus de "El Carmen", 21071 Huelva, Spain
[c]Hasselt University, Institute for Materials Research (IUMAT), Metabolomics and Advanced Solid State NMR Group (MAS-NMR), Martelarenlaan 42, B-3500 Hasselt, Belgium
[d]imec, IUMAT, Wetenschapspark 1, B-3590 Diepenbeek, Belgium
[e]Institut Universitaire de France (IUF), Paris, F-75231, France

Open Access Article. Published on 28 April 2026. Downloaded on 6/2/2026 10:49:01 AM. This article is licensed under a Creative Commons Attribution-NonCommercial 3.0 Unported Licence.

Open Access Article. Published on 28 April 2026. Downloaded on 6/2/2026 10:49:01 AM. This article is licensed under a Creative Commons Attribution-NonCommercial 3.0 Unported Licence.

amounts of aromatic compounds, which could be suitable as HCP precursors.

The present study thus aims to develop and optimize MS of HCPs using CTPs as precursors, thereby contributing to the "turning waste into resource" concept of the Circular Economy. The intrinsic nature of the MS process would allow substantial savings in energy, time and reagents, and the synthesis is "greener" than conventional synthesis methods as no solvents are required. In order to gain insight into the MS process, considering that CTPs are mainly composed of aromatic substances, a first study was carried out using benzene as a model HCP precursor. Then, based on these results, the synthesis of CTP-derived HCPs was studied by modifying synthesis parameters such as reaction time and precursor/catalyst/crosslinker molar ratio. The HCPs obtained were characterized by thermogravimetric analysis/mass spectrometry (TGA/MaSp) and nitrogen adsorption–desorption at −196 °C. Finally, given the hydrophobic nature of the HCP's aromatic chains, which could favor the adsorption of many pollutants in wastewater, from metals to organic compounds such as dyes,[10,15–18] their suitability for wastewater remediation was tested by measuring their methylene blue adsorption capacity as a proof of concept.

2 Materials and methods

2.1 Materials

The coal tar products (CTPs), namely, chrysene oil, wash oil, distilled coal tar pitch (DCTP), creosote B (hereafter referred to as creosote only), phenolic oil, naphthalene oil and depleted naphthalene oil (DNO) were all produced and provided by *Bilbaína de Alquitranes S.A* (BASA, Spain). Before use, all the CTPs were heated to 15 °C above their crystallization temperature and stirred for at least 1 h to ensure homogenization. Benzene (99.8% purity), used as a reference monomer, iron chloride ($FeCl_3$, 99.6% purity), used as a catalyst, 1,2-dichloroethane (DCE, 99% purity), used as a solvent, dimethoxymethane, also called formaldehyde dimethyl acetal (FDA, 93% purity), used as crosslinker, were obtained from Sigma Aldrich. Toluene and methanol used to wash the HCPs produced were purchased from Carlo Erba, and ethanol was obtained from VWR.

2.2 Mechanosynthesis of HCPs

The FC reaction was carried out in a 250 mL stainless steel ball-milling bowl using 50 balls of 1 cm diameter. Precursor, catalyst and crosslinker were added to the bowl under an Ar atmosphere. Because FDA is highly volatile, it was added last; immediately afterward, the bowl was sealed and placed in a PM 100 planetary mill (Retsch), ensuring a hermetic seal to prevent reagent evaporation. The mill's rotational speed was fixed at 500 rpm and different reaction times and precursor/catalyst/crosslinker molar ratios were tested. Some MS tests were also carried out using a MM 500 nano mixer mill (Retsch) at a vibration frequency of 30 Hz, with a 50 mL ZrO_2 bowl using 10 ZrO_2balls of 1 cm diameter. To maintain the same volume ratio between reagents and bowl, the amounts of reagents added to the ZrO_2 bowl were 1/5 of those added to the stainless-steel system. In addition, several SC reactions were performed, for which no crosslinker was added to the precursor/catalyst mixture.

Once the MS reaction was completed, the HCPs were recovered and purified following the procedure reported by Lee *et al.*[10] Briefly, the HCPs were washed several times, first with ethanol and then methanol, followed by a 24 h Soxhlet extraction using a toluene/ethanol mixture with a weight ratio of 32/68, in order to remove unreacted compounds and catalyst. Afterwards, the sample was dried by heating under vacuum at 80 °C for 24 h. The reaction yield (wt%) was calculated using the following equation:

$$\text{Reaction yield} = 100 \times \frac{m_{\text{HCP}}}{m_{\text{p}} + m_{\text{cross}}}$$

were m_{HCP} is the mass of HCP recovered, while m_{p} and m_{cross} are respectively the mass of the precursor and the mass of the crosslinker used in the synthesis.

2.3 Characterization

The different CTPs kindly provided by BASA were analyzed by high-performance liquid chromatography in an Agilent Technologies gas chromatograph Model 7890N coupled to a mass spectrometer selective detector 5975C equipped with a 7693A autosampler. The chemical composition of the CTPs is given in Tables S1 to S7. From these data, the molecular weight of each CTP, $M_{\text{W,CTP}}$, was calculated by:

$$M_{\text{W,CTP}} = \sum_i A_i \times M_{\text{W},i}$$

were i refers to the compound, A_i is its abundance, and $M_{\text{w},i}$ is its molecular weight.

Fourier-transform infrared spectroscopy (FTIR) was carried out in the 4000–600 cm^{-1} range, with a resolution of 4 cm^{-1} using a Spotlight 400 instrument (PerkinElmer) equipped with an attenuated total reflectance imaging accessory for sampling. Thermogravimetric (TG) analysis coupled to mass spectrometry (MaSp) was performed in a STA 449F3 Jupiter microbalance coupled to a QMS 403 D mass spectrometer (Netzsch). The tests were conducted under Ar atmosphere, from room temperature to 900 °C, a temperature maintained for 30 min. To analyze the TG results, the derivative of the mass loss ($D(-\Delta M)$) curve was calculated, leading to peaks corresponding to the different thermal events. N_2 adsorption–desorption isotherms at −196 °C for HCPs were obtained using a Belsorp Max II apparatus (Microtrac). Prior to N_2 adsorption–desorption analysis, the samples were outgassed at 60 °C for at least 48 h under secondary vacuum. The BET area (A_{BET}) was calculated using the N_2 adsorption isotherms. Elemental analysis (EA) was also performed using a Vario EL cube analyzer (Elementar) to determine carbon, hydrogen, nitrogen, sulfur and oxygen contents (wt%) after burning ~2 mg of each sample and separating the gases generated through a chromatographic column.

Selected samples were analyzed using ^{13}C MAS (magic angle spinning) solid-stated NMR spectroscopy. The spectra were acquired at ambient temperature on a ECZL-400 G 400 MHz

© 2026 The Author(s). Published by the Royal Society of Chemistry

Open Access Article. Published on 28 April 2026. Downloaded on 6/2/2026 10:49:01 AM. This article is licensed under a Creative Commons Attribution-NonCommercial 3.0 Unported Licence.

spectrometer (9.4 T, Jeol) equipped with a 3.2 mm HXMAS probe. MAS was performed at 18 kHz and the aromatic signal of hexamethylbenzene was used to calibrate the carbon chemical shift scale (132.1 ppm). Acquisition parameters used were: a spectral width of 70 kHz, a ^{13}C 90° pulse length of 2.9 μs, an acquisition time of 18 ms, a recycle delay time of 60 s, and at least 7000 scans. High-power proton dipolar decoupling during the acquisition time was set to 70 kHz.

In addition, the selected samples were analyzed using the double-shot thermal desorption pyrolysis technique combined with gas chromatography/mass spectrometry (TD-PY-GC/MS). The analysis was performed with an EGA/3030-D Multi-Shot Pyrolyzer (Frontier Laboratories LTD) and a Trace 1300 gas chromatograph (Thermo Scientific) equipped with DB-5MS capillary column (30 m length, 0.25 mm I.D., film thickness 0.25 μm, Agilent Technologies) coupled to an ISQ 7000 single quadrupole mass spectrometer (Thermo Scientific). The samples were weighed (0.31 mg 'Creosote 1/2/2 MS 5 min', and 0.41 mg 'Creosote 1/6/2 MS 5 min') in an Eco-Cup SF (PY1-EC50F, Frontier Laboratories LTD) and transferred into the pyrolysis module, where they are subjected to a two-step temperature program. During the first step (TD), the initial temperature of the pyrolysis module is set to 150 °C and heated at a rate of 25 °C min^{-1} to a final temperature of 300 °C with a hold time of 4 minutes, after which the released volatiles are analyzed *via* GC/MS, yielding a TD chromatogram. After the TD, the residual fraction is heated for 0.2 minutes at 600 °C in a second step (PY) from which the pyrolyzates are also analyzed by GC/MS, resulting in a PY chromatogram (pyrogram). The volatiles and pyrolyzates from the TD and PY stages are introduced into the capillary column with a 1/80 split, where they are concentrated at the front of the column by cryo-focusing with the Micro Jet Cryo-Trap module (MJT-1035E, Frontier Laboratories LTD) using liquified nitrogen at −195 °C, until the end of the TD and PY programs. Hereafter, the temperature of the column was maintained at 35 °C for 1 minute and raised to 320 °C at a rate of 10 °C min^{-1} and a final hold time of 2.5 minutes. The injection port was set at 300 °C and the mass spectrometer transfer line at 280 °C. Helium was used as carrier gas and the flow rate was set at 1 mL min^{-1}. The mass spectrometer was operated in electron ionization mode with 70 eV at a source temperature of 300 °C and a mass range of 33–550 m/z with a scan time of 0.2 s. Data processing was performed using Chromeleon 7.3 (Thermo Scientific).

Methylene blue (MB) adsorption tests were performed by contacting 5 mg of sample with 7 mL of a solution containing 200 ppm of methylene blue in distilled water. The suspensions were stirred vigorously with a magnetic bar for 30 min at 20 °C, after which they were filtered and diluted, and absorption at a wavelength of 663 nm was measured in a Lambda 35 UV/vis spectrophotometer (PerkinElmer). The results are reported in milligrams of MB removed per g of sample (mg_{MB} g_s^{-1}). The HCPs were filtered after the MB removal tests, washed thoroughly with ethanol and dried at 60 °C overnight for reuse. This process was repeated for four cycles to assess reusability. The potential release of harmful components from the HCPs was finally evaluated by immersing the HCPs in 40 mL of distilled water. The dispersion was stirred using a planetary shaker for 96 hours at 50 °C and 50 rpm. Afterward, the UV-vis absorption profile was acquired in the range of wavelengths from 200 to 700 nm.

3 Results and discussion

3.1 HCPs from different coal tar products (CTPs)

Seven different CTPs, namely chrysene oil, wash oil, distilled coal tar pitch (DCTP), creosote, phenolic oil, naphthalene oil and depleted naphthalene oil (DNO), were tested as precursors for HCP synthesis. Two precursor/catalyst/crosslinker molar ratios of 1/2/2 and 1/6/2 were used for HCP synthesis, with a fixed reaction time of 5 min using a planetary mill with a stainless-steel bowl and balls. These specific catalyst ratios were selected based on the results previously reported in studies of MS-synthesized HCPs.[10]

Following the milling and washing steps, the liquid CTPs transformed into a solid brown powder, which is an indication of successful crosslinking, see Fig. 1A. Reaction yields remained between 40 and 50 wt% for all CTPs. From TG analysis, Fig. 1B and C, important differences were found. For samples with a molar ratio of 1/2/2, all curves exhibited a main thermal event at around 500 °C. This behavior is similar to that observed for solvent-based HCPs.[7] For a molar ratio of 1/6/2, a higher mass loss ($-\Delta M$) is observed during the first thermal event at a lower temperature, possibly indicating a greater presence of branched chains with low thermal stability. It is also noteworthy that the values of the residual weight fraction at 900 °C (R_{900}) were strongly influenced by the catalyst content. For example, a precursor/catalyst molar ratio of 1/6 resulted in an increase of around 10 wt% in the R_{900} value compared with the molar ratio 1/2 (see Fig. 1B and C), and, in all cases, chrysene oil provided the HCP with better thermal stability, exhibiting the highest R_{900}.

Furthermore, significant differences were observed in the A_{BET} values obtained from N_2 adsorption–desorption measurements depending on the precursor used, as shown in Fig. 1D and E. Specifically, DCTP and chrysene oil failed to provide HCPs with A_{BET} higher than 60 m^2 g^{-1}, whatever the molar ratio. For phenolic oil, the use of a high catalyst content resulted in a material with an A_{BET} of only 20 m^2 g^{-1}, while for a 1/2 ratio it reached a value of 180 m^2 g^{-1}. In the case of wash oil, for a 1/6/2 ratio, the HCPs had A_{BET} values slightly higher than 100 m^2 g^{-1}. Notably, creosote led to an A_{BET} of approximately 160 m^2 g^{-1} for both catalyst contents, the highest value among all the CTPs for a 1/6/2 ratio, while for a 1/2/2 ratio, the highest A_{BET} of 320 m^2 g^{-1} was obtained using DNO as a precursor. Based on these results, creosote and DNO were selected for further study and characterization, described in detail in the following sections.

3.2 Benzene-derived HCPs as model

Before studying in more detail, the synthesis of creosote- and DNO-derived HCPs, a study using benzene as a model HCP precursor was first carried out to better understand the influence of MS parameters. This study was made using a benzene/

Open Access Article. Published on 28 April 2026. Downloaded on 6/2/2026 10:49:01 AM.
This article is licensed under a Creative Commons Attribution-NonCommercial 3.0 Unported Licence.

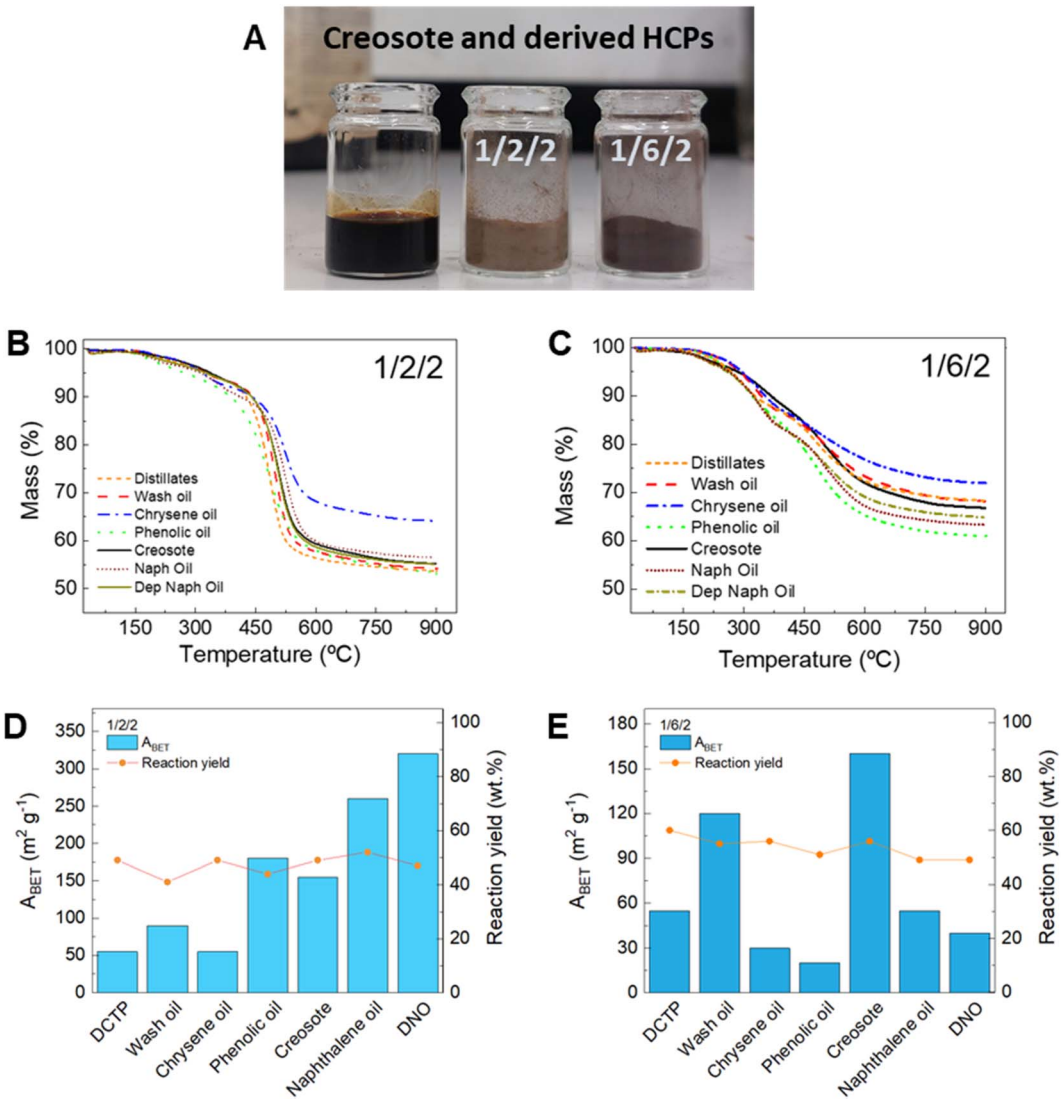

Fig. 1 (A) From left to right, creosote and its derived HCPs using a precursor/catalyst/crosslinker molar ratio of 1/2/2 and 1/6/2. TG analysis (mass loss, $-\Delta M$) of HCPs formulated using different CTPs and precursor/catalyst/crosslinker molar ratios: (B) 1/2/2, and (C) 1/6/2. A_{BET} and reaction yields of CTP-derived HCPs at molar ratios: (D) 1/2/2 and (E) 1/6/2.

catalyst/crosslinker molar ratio of 1/6/2, varying the reaction time from 3 to 60 min, and using either a planetary mill or a mixer mill.

FTIR analysis was used to identify the main chemical bonds that form the structure of the obtained HCPs, as well as to quantify certain differences based on the intensity of the observed peaks. Fig. S1A and B shows the FTIR spectra of the benzene-derived HCPs obtained using the planetary mill, BPM*t* (*t*, reaction time in minutes). The first bands in the FTIR spectra appeared around 3020, 2973, and 2925 cm^{-1}. The latter two are related to CH_2 stretching, while these same units were also observed in bending at around 1500 and 1300 cm^{-1}.[19] The first peak at 3020 cm^{-1} was attributed to the hydrogen stretching vibration in aromatic rings.[20–22] Compared with the FTIR spectrum of benzene (Fig. S1C), the reduction in the amount of =C–H units and the presence of new CH_2 bonds can be observed in this range, confirming the cross-linking.

The peaks observed between 1700 and 1435 cm^{-1} were attributed to the –C=C– units of the benzene structure,[21–23] which are shifted with respect to the main –C=C– stretching vibration of the pristine molecule (1478 cm^{-1}, see Fig. S1C). Intense signals were also found around 700 cm^{-1}, corresponding to the out-of-plane vibration of aromatic C–H,[24] once again, slightly offset from that of benzene. It is important to note that the FTIR spectra were normalized by the intensity of the CH_2 stretching vibration at 2925 cm^{-1}, so it is clear in Fig. S1B that the longer the reaction time, the more –C=C– units are present (increased intensity of peaks in the range 1700–1435 cm^{-1}), suggesting a higher degree of crosslinking. The same behavior was observed when analyzing benzene-derived HCPs obtained using the mixer mill, BMM*t* (*t*, reaction time in minutes), see Fig. S1D. Similar FTIR profiles were obtained for materials synthesized using either the planetary

© 2026 The Author(s). Published by the Royal Society of Chemistry

Open Access Article. Published on 28 April 2026. Downloaded on 6/2/2026 10:49:01 AM.
This article is licensed under a Creative Commons Attribution-NonCommercial 3.0 Unported Licence.

mill or the mixer mill, as shown for BPM30 and BMM30 materials in the inset of Fig. S1C.

On the other hand, for BPM*t*, TG analysis showed that very similar profiles are obtained regardless of reaction time, see Fig. 2A and Table S8. Three main thermal events take place during TG analysis (see bottom of Fig. 2A), the first being centered around 297–327 °C and the second and third around 477–498 °C and 539–553 °C, respectively. In general, as mass loss during the third thermal event decreased, an increase in the thermal stability of the HCP produced was observed, corresponding to a higher R_{900}.

To evaluate the various compounds released during these events, MaSp was coupled with the TG apparatus. Fig. 2C shows an example of the release of ethyl and methoxy moieties (molar mass of 29 and 31 g mol^{-1}, respectively) from sample BPM5, which occurs only during the first thermal event. This suggests the elimination of small branched chains, a likely consequence of incomplete cross-linking that results in FDA molecules being linked to only one benzene molecule (see inset in Fig. 2C). Thermal degradation of similar HCPs obtained by solvent-based FC reactions shows a single main event, suggesting that partial branching does not occur or occurs at a much lower level when solvents are used.[7] This may be attributed to the more homogeneous distribution of components in solution, which promotes better interaction between them and thereby reduces the likelihood of partial branching. On the other hand, methyl

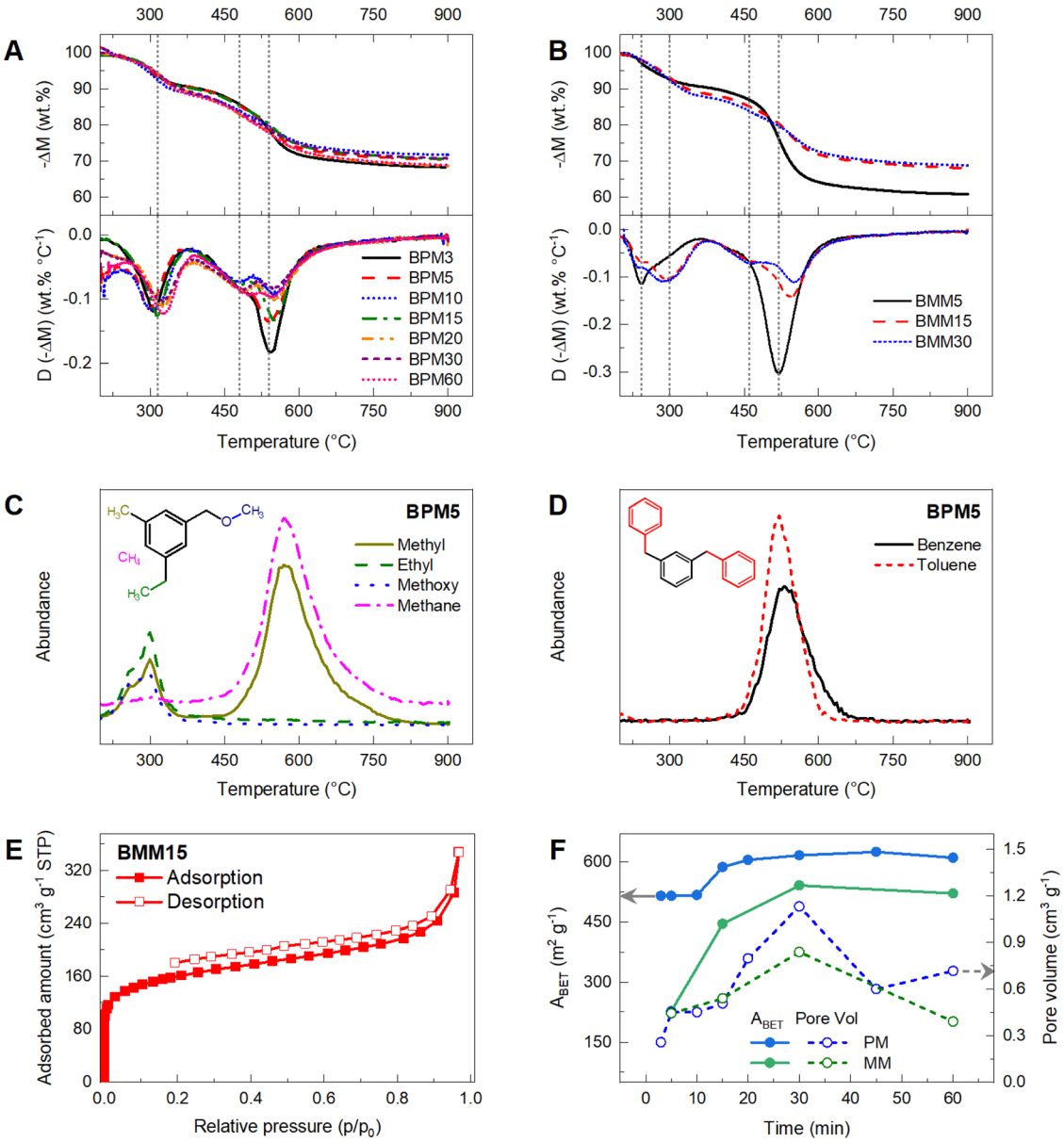

Fig. 2 TG analysis (mass loss (−Δ*M*) and its derivative (*D*(−Δ*M*)) of benzene-derived HCPs synthesized using: (A) a planetary mill, BPM*t*, and (B) a mixer mill, BMM*t*, with *t* standing for milling time in minutes. Release of (C) methyl, ethyl, methoxy, methane, (D) benzene and toluene moieties, measured by MaSp. (E) N_2 adsorption–desorption isotherms of a benzene-derived HCP, BMM15. (F) A_{BET} and pore volume obtained at different reaction times for benzene-derived HCPs prepared by using a planetary mill (PM) and a mixer mill (MM).

© 2026 The Author(s). Published by the Royal Society of Chemistry

Open Access Article. Published on 28 April 2026. Downloaded on 6/2/2026 10:49:01 AM. This article is licensed under a Creative Commons Attribution-NonCommercial 3.0 Unported Licence.

units (15 g mol^{-1}) are released in all events, probably as an initial loss of CH_3- moieties attached to easily accessible benzenes, which is continued by further degradation of the HCP structure during the second and third events. On the contrary, methane is mainly released during the second and third events, possibly as a secondary reaction of the C–C breakage of the main HCP structure. As can be observed in Fig. 2D, benzene and toluene moieties (78 and 92 g mol^{-1}, respectively), the main units of the HCP structure, are only released at the highest temperatures, due to the C–C bond breakage in the crosslinked network. This suggests a partial loss of the HCP structure at these temperatures, even though R_{900} is still considerably high (~70 wt%).

The behavior for BMM*t* series of samples is more complex (see Fig. 2B). For instance, BMM5 exhibits a considerably lower R_{900}, 61 wt%, and two main thermal events at 243 and 520 °C. As reaction time increases, the first event broadens and shifts to a higher temperature, 300 °C. In addition, the single thermal event observed at 520 °C for BMM5, which results in a mass loss of 30 wt%, splits into two thermal events, at 460 and 551 °C for BMM15 and BMM30, which only result in a mass loss of 19 wt%, hence the increase in R_{900}. The lower thermal stability of BMM5, which is probably a consequence of poor cross-linking, is not observed for BPM5 or BPM3. This difference could be attributed to the combination of denser ball and bowl material (stainless steel) and the operating mechanism of a planetary mill. Indeed, the planetary mill typically delivers more energy to the system than mixer mills,[25] which could facilitate the development of a stable structure even with a shorter reaction time.

Fig. 2E shows the N_2 adsorption–desorption isotherm for sample BMM15, provided as an example. Consistent with observations for other benzene-derived HCPs, both solvent- and MS-based, the isotherms correspond to a combination of type Ib and II isotherms, according to the IUPAC classification.[19,26] Thus, the presence of micropores is confirmed by the high uptake at low relative pressure ($p/p_0 < 0.05$), while the presence of large mesopores is suggested by the increase in adsorption at high relative pressure ($p/p_0 > 0.90$). The isotherm also show hysteresis at low-relative pressure, which could be attributed either to diffusion problems within the microporous structure,[26] or to the presence of a flexible porous structure capable of swelling. Similar phenomena have been reported for HCPs previously.[7]

The study of different reaction times under different milling protocols provided some very interesting outcomes. An initial trend of increasing A_{BET} was observed in both cases, with the BPM*t* series reaching a plateau at high reaction times (see Fig. 2F), in agreement with results reported by Krusenbaum *et al.*[27] As mentioned above, a reaction time of 5 min seems too low to obtain an HCP with a high level of crosslinking using the mixer mill (ZrO_2 bowl and balls), which does not provide enough energy to the system under the selected conditions. This was corroborated by the N_2 adsorption results since a low A_{BET} of 228 m^2 g^{-1} was obtained for BMM5. Increasing the reaction time to 15 min doubled the A_{BET}, reaching 445 m^2 g^{-1}. Furthermore, after 30 min of reaction time, A_{BET} increased to 541 m^2 g^{-1}, and this A_{BET} value was fairly maintained after 60 min. Moreover, due to the inherently higher energy provided by the use of stainless steel as a milling material, only 3 min were sufficient to achieve an A_{BET} close to that obtained after 30 min in the ZrO_2 bowl (515 m^2 g^{-1}). These findings are consistent with tests conducted by Gratz *et al.* using different ball milling materials at the same reaction times.[25] A_{BET} remained unchanged after 5 and 10 min of reaction time, however, from 15 min onwards, a sudden increase in A_{BET} was observed, reaching a maximum of around 615 m^2 g^{-1} after 30–60 min. Comparison of our results with those obtained for benzene-derived HCPs by Lee *et al.*[10] leads to the conclusion that a higher ratio between ball volume and bowl volume, together with a higher rotation speed, significantly potentiates cross-linking, since only 5 min were necessary to achieve higher A_{BET} values than those obtained here after 20–60 min. Contradictory results were obtained regarding the effect of ball size, with some authors observing a positive influence of increasing ball size,[25,28] while Krusenbaum *et al.*[29] found that the maximum A_{BET} was achieved when using 10 mm balls. In their study, changing the ball size, either by increasing or decreasing their dimensions while keeping the weight constant, led to lower A_{BET} values.

A general trend towards increased pore volume was observed with longer reaction times. However, in the BPM*t* series, a substantial decrease in pore volume was observed after a reaction time of 60 min, reaching a value close to that obtained at 20 min. This suggests that further improvements are not to be expected by increasing reaction time. Even though A_{BET} was closely maintained over the reaction time range of 3–10 min, the pore volume significantly increased, from 0.26 to 0.45 cm^3 g^{-1}. The pore volume continued to increase, almost linearly, up to a reaction time of 30 min, reaching 1.13 cm^3 g^{-1}, before decreasing thereafter, as previously mentioned. Nevertheless, this maximum pore volume is higher than that reported for other solvent-based HCPs[7] and the one reported by Lee *et al.*[10] for their optimal benzene-derived HCP. For the BMM*t* samples, a significant initial increase in pore volume was observed with a reaction time of up to 30 min, reaching pore volumes as high as 0.84 cm^3 g^{-1}. However, a further increase in reaction time to 60 min resulted in a reduction in pore volume down to 0.39 cm^3 g^{-1}. The presence of small branches suggested by TG/MaSp analysis could explain the lower porosity development observed for BMM-*t* HCPs compared to a solvent-based benzene-derived HCP.[7]

3.3 HCP structure

In Section 3.1, it was shown that the catalyst content significantly changes the thermal stability of the obtained materials (see TG curves in Fig. 2). To gain more insights into the possible structure of the coal tar-derived HCPs, ^{13}C MAS solid-state NMR analysis and TD-PY-GC/MS analyses were carried out on two samples, namely creosote MS 5 min 1/2/2 and 1/6/2. Both samples exhibited similar NMR spectra, see Fig. S2 (and Table S9 for the group contributions), with a high content of aromatics (>70%) and similar contributions from methoxy groups (~2%). However, the 1/6/2 sample contains more alkoxy

 © 2026 The Author(s). Published by the Royal Society of Chemistry

Open Access Article. Published on 28 April 2026. Downloaded on 6/2/2026 10:49:01 AM. This article is licensed under a Creative Commons Attribution-NonCommercial 3.0 Unported Licence.

CH_2–O carbons. Indeed, small yet distinct differences were observed in the 60–90 ppm region, with internally normalized contributions of 5.7% for the 1/6/2 sample and 2.9% for the 1/2/2 one. A small difference was also observed in the carbonyl region, where the contributions from these groups are 2.7 and 1.5% for the HCP obtained using a 1/6/2 and a 1/2/2 ratio, respectively.

Furthermore, the 1/6/2 sample exhibited higher gas release than the 1/2/2 sample during the first decomposition step at 300 °C in TD-PY-GC/MS analysis. This finding is consistent with TGA results. Additionally, this analysis revealed that the 1/6/2 sample has a more complex volatile product slate. This profile includes several oxygenated and chlorinated products in addition to the dominant toluene signal. During the second decomposition step at 600 °C, both samples exhibited a complex mixture of decomposition products, rich in polyaromatic compounds and alkyl-substituted analogues. The chromatograms from TD-PY-GC/MS analyses and a detailed list of the decomposition products for both samples are provided in Fig. S3 and Tables S10 to S13, respectively. Furthermore, the PY-GC/MS analysis showed that the creosote-derived HCPs' decomposition products include larger molecules, such as anthracene, phenanthrene, and pyrene (see Tables S10–S13), in higher proportions than in the original creosote (see Table S5). This also indicates that polymerization through crosslinking was achieved.

Considering the results from these characterization techniques and the results from previous sections, a structure of the creosote-derived HCPs is proposed and schematized in Fig. 3. This structure consists of a main polyaromatic core formed from the crosslinking of creosote's main compounds (*e.g.*, anthracene, acenaphthene, naphthalene, and fluorene; see Table S5) and smaller molecules that are partially crosslinked (colored in Fig. 3). Using a larger amount of catalyst leads to a higher presence of alkoxy branches compared to the main structure, as evidenced by the NMR and TD-GC/MS results.

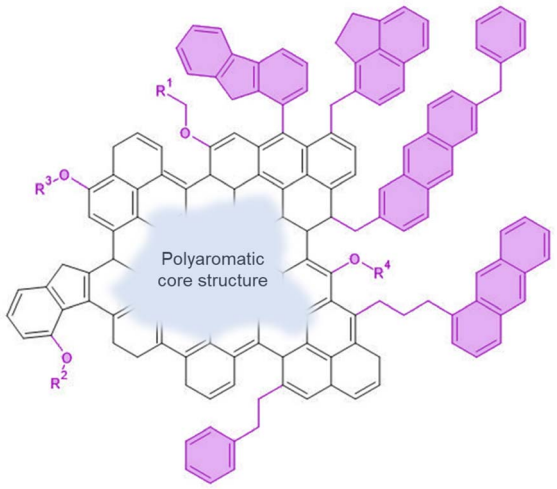

Fig. 3 Proposed structure of the creosote-derived HCP based on results from TGA, ^{13}C MAS solid-state NMR and TP-PY-GC/MS analyses. A larger amount of catalyst during synthesis leads to a higher presence of the colored branches.

In the following sections, the synthesis of creosote- and DNO-derived HCPs is studied in detail, changing different parameters such as the reaction time, the catalyst and the crosslinker content. The study of these parameters aims to optimize the synthesis process to obtain a highly porous HCP.

3.4 Creosote-derived HCPs

Firstly, the influence of catalyst content and reaction time was studied in more detail. Three different precursor/catalyst/crosslinker molar ratios were tested, with the catalyst content ranging from 2 to 6, *i.e.*, 1/[2–6]/2, with reaction times between 5 and 60 min. In a second approach, the effect of crosslinker content was evaluated, ranging from 0 to 2, with a fixed amount of catalyst, *i.e.*, 1/6/[0–2].

3.4.1 Effect of catalyst content and reaction time. Creosote-derived HCPs exhibited very similar FTIR spectra to those of the benzene-derived synthesis, indicating the formation of an aromatic-based structure, see Fig. S4. The presence of –C=C– units, forming a well-developed complex structure, was again confirmed in the 1700–1441 cm^{-1} range, as was the reduction in the intensity of the peak of aromatic = C–H units centered around 750 cm^{-1}.[21] In comparison, the intensity of –C=C– units in creosote-derived HCPs synthetized with a 1/2/2 molar ratio showed a general tendency to increase with reaction time, while the opposite behavior was observed for –C–H units, confirming precursor cross-linking, see Fig. S4A. However, observing the sample after 60 min of milling, the peak at 1695 cm^{-1} was significantly reduced, while the peak at 750 cm^{-1} showed a high intensity. In the case of the 1/4/2 molar ratio, the most significant feature was that at 60 min, the reduction in C–H units (751 cm^{-1} peak) was much more intense than for any other sample in the series, see Fig. S4B. In contrast, the 1/6/2 molar ratio showed the highest intensity for double-bond structural units at 30 min (peaks in the range 1700–1441 cm^{-1}), see Fig. S4C.

Creosote-derived HCPs were subjected to TG analysis and the results are shown in Fig. 4A–C, S5 and Table S14. For the molar ratio 1/2/2, all samples in this series showed a minor thermal event around 205 °C, resulting in mass losses from 1 to 4 wt% (Fig. S5D and Table S14). For reaction times up to 15 min, another small thermal event is observed at approximately 350 °C, which vanished for reaction times exceeding 30 min. Finally, the primary thermal event at around 508 °C resulted in the highest mass loss for all samples, with a noticeable shift towards higher temperatures as R_{900} increased. In this case, the longer the reaction time, the higher the R_{900} values, *i.e.*, the better the thermal stability (inset in Fig. S5D and Table S14). However, after a reaction time of 60 min, the sample evidenced a significantly greater mass loss, with the lowest R_{900} among the series. For the 1/4/2 molar ratio, the mass loss during the first thermal event, around 209 °C, increased with reaction time, from 0 up to 9 wt%, and a second thermal event at around 333 °C was also observed, with greater significance in samples synthesized using shorter reaction times (Fig. S5D and Table

Open Access Article. Published on 28 April 2026. Downloaded on 6/2/2026 10:49:01 AM.
This article is licensed under a Creative Commons Attribution-NonCommercial 3.0 Unported Licence.

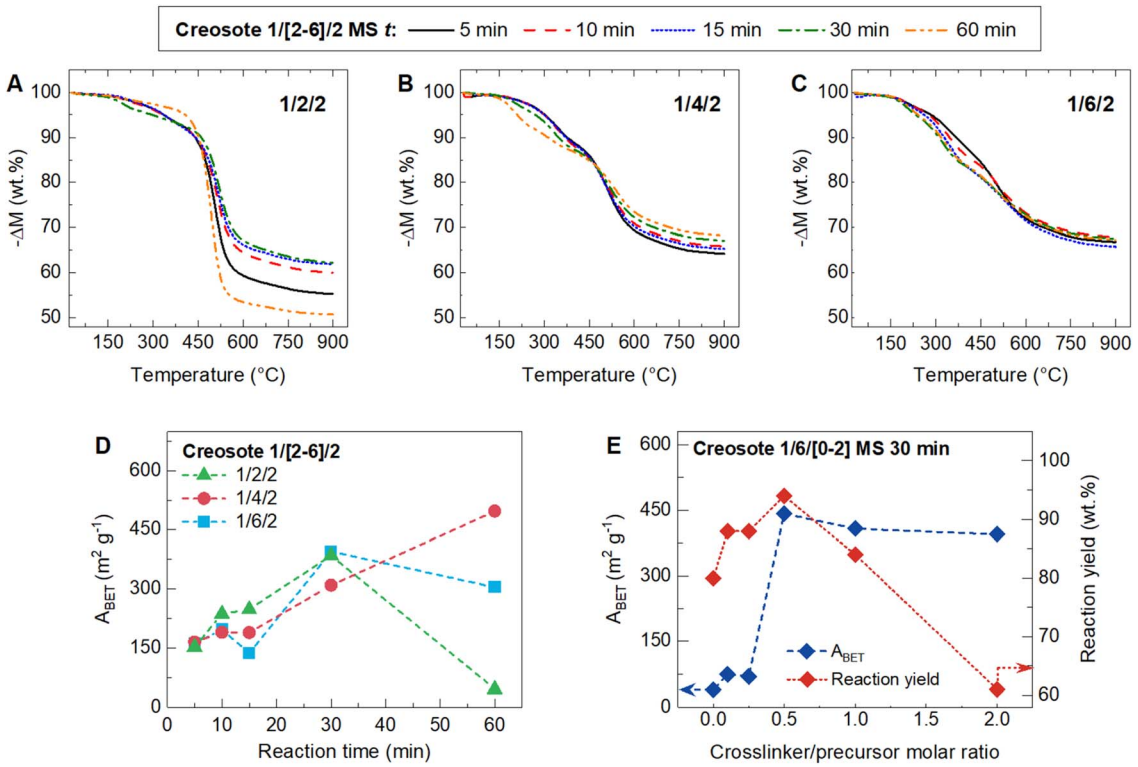

Fig. 4 TG analysis mass loss curves of creosote-derived HCPs synthesized using a precursor/catalyst/crosslinker molar ratio of (A) 1/2/2, (B) 1/4/2, and (C) 1/6/2, and reaction times from 5 to 60 min. (D) A_{BET} for creosote-derived HCPs using different catalyst contents (1/[2–6]/2 molar ratio) as a function of reaction time. (E) A_{BET} for creosote-derived HCPs as a function of crosslinker content, for a fixed catalyst content (1/6/[0–2] molar ratio).

S14). Finally, a slight improvement in the thermal stability was noted with increasing reaction time, even after 60 min (inset in Fig. S5D and Table S14), the differences in R_{900} are mostly due to the mass loss during the main thermal event (~518 °C). Concerning the 1/6/2 molar ratio, all samples showed similar thermal stability at 900 °C (inset in Fig. S5D and Table S14), as evidenced by the minimal variation in R_{900} values. However, some differences can be observed on closer inspection of the different thermal events (Fig. S5D and Table S14). During the first thermal event, ~210 °C, the mass loss changes by only 3 to 5 wt% for the lowest and highest reaction times, respectively. In contrast, during the second thermal event, the mass loss exhibits a more significant increase ranging from 8 to 15 wt% after 5 and 15 min of reaction time, before decreasing to 12 wt% for longer reaction times. As with the other two series of materials, the highest mass loss values were observed during the third thermal event. However, it is worth mentioning that increasing the catalyst content amplified the significance of the first and second thermal events occurring between 200 and 350 °C (Fig. S5D and Table S14). This observation suggests that increasing the catalyst content led to the formation of an HCP structure with different types of bonds characterized by lower stability at moderate temperatures. This finding aligns with the proposed structure of the HCP illustrated in Fig. 3A. Interestingly, once these poorly heat-stable bonds are broken, the remaining structure exhibits better thermal resistance at higher temperatures with increasing catalyst content, as evidenced by the R_{900} values.

Elemental analysis of selected HCPs was performed, namely those with molar ratios 1/[2–6]/2 and a fixed reaction time of 30 min. As shown in Table S15, carbon and hydrogen contents decreased with increasing catalyst concentration, while oxygen content increased. These findings are, again, in line with the proposed structures illustrated in Fig. 3, which are further supported by TG/MaSp analysis, suggesting that an increase in catalyst content leads to a greater presence of partially crosslinked FDA units.

To further investigate the behavior observed during the TG analysis, the samples were also studied by MaSp coupling, as was done for benzene-derived HCPs. In the case of methane and methoxy units, for molar ratios 1/2/2 and 1/4/2, shorter reaction times were associated with increased release of both compounds, whereas lower release was observed between 15 and 60 min, see Fig. S6A and C. However, when the catalyst content was increased, as seen for the 1/6/2 molar ratio, the sample subjected to a reaction time of 60 min showed the highest release of both methoxy and methane units, see Fig. S6E. As mentioned above, a greater presence of methoxy units may indicate incomplete crosslinking, suggesting that long reaction times are necessary when using a low catalyst content. Meanwhile, for a 1/6/2 molar ratio, an optimum seems to be reached after 30 min of reaction time, beyond which some

© 2026 The Author(s). Published by the Royal Society of Chemistry

Open Access Article. Published on 28 April 2026. Downloaded on 6/2/2026 10:49:01 AM. This article is licensed under a Creative Commons Attribution-NonCommercial 3.0 Unported Licence.

structural damage might occur. This aligns with findings reported for benzene-derived HCPs by Lee *et al.*, where relatively long reaction times led to similar observations.[10]

The release of benzene and toluene was also examined, but due to the minimal release of such molecules and the fact that the precursor consisted of a mixture of aromatic compounds, the MaSp signal was not consistent. Nonetheless, a general trend emerges from Fig. S6B, D and F: higher reaction times resulted in lower release of both compounds, likely indicating the formation of a stronger structure. In order to identify other high-molecular weight compounds released during the thermal degradation of HCPs, MaSp analysis was extended to 300 *m*/*z*. However, no significant peaks were observed beyond 206 *m*/*z*. Interestingly, only samples synthesized using a 1/2/2 molar ratio displayed the release of heavier compounds after 60 min of reaction, while those synthesized using 1/4/2 and 1/6/2 molar ratios showed no such releases, see Fig. S7A. This suggests that, once the small branches are eliminated, a stronger structure can be obtained by increasing the catalyst content, as already anticipated by the higher R_{900} from the TG analysis. For shorter reaction times, as shown in Fig. S7B, the detection of naphthalene and another peak at 142 *m*/*z* was noticeable for sample 1/4/2. Additionally, fluorene, anthracene, phenantrene and 2-methylphenantrene were detected by analyzing the spectra of the 1/2/2 series of materials. This once again confirms the lower thermal stability of the structure created using this lower molar ratio.

On the other hand, the N_2 isotherms of creosote-derived HCPs showed similar profiles regardless of catalyst content, displaying high uptake at both low and high relative pressures, as shown in Fig. S8A for a fixed reaction time of 30 min. From the N_2 isotherms, A_{BET} was calculated and results are presented in Fig. 4D, where a maximum value is observed at 30 min reaction time for both 1/2/2 and 1/6/2 molar ratios, with 385 and 395 $m^2\ g^{-1}$, respectively. For the 1/4/2 ratio, the maximum value was obtained at 60 min reaction time, 497 $m^2\ g^{-1}$. Interestingly, despite the significant increase in catalyst content, A_{BET} remained in the 140–250 $m^2\ g^{-1}$ range for reaction times between 5 and 15 minutes. Notably, significant changes in A_{BET} values were only observed after 30 min of reaction time. However, it is worth noting that the maximum A_{BET} value obtained using creosote as a precursor was 497 $m^2\ g^{-1}$, which is approximately 20% lower than that for benzene-derived HCPs (maximum A_{BET} of 615 $m^2\ g^{-1}$).

3.4.2 Effect of crosslinker content. Creosote-derived HCPs, synthesized with fixed reaction time and varying crosslinker contents, were subjected to TG/MaSp analysis, and the results are reported in Fig. S9 and summarized in Table S14. Fig. S9B shows that losses during the first and second events (at ~205 and ~310 °C) increased with crosslinker content, resulting in a lower R_{900} of 68 wt% (see also Table S14). However, it is worth noting that a molar ratio of 1/6/1 already led to a reduced mass loss during the second thermal event. Despite the occurrence of a fourth thermal event at a higher temperature, approximately 730 °C, for molar ratios of 1/6/0.5 and 1/6/0, these ratios yielded creosote-derived HCPs with the highest final thermal stability of the series, with R_{900} values of 73 and 74 wt%, respectively. MaSp analysis, shown in Fig. S9C, evidenced that an increase in crosslinker content corresponded to greater release of methane, in accordance with the anticipated greater amount of methylene bridges that could be formed. Similarly, a comparable pattern can be observed with methoxy units, attributed to a greater presence of partially crosslinked branches when a higher crosslinker content is employed. However, benzene and toluene release was minimal in this case, making it challenging to identify a discernible trend from the spectra, as shown in Fig. S9D.

Surprisingly, despite previous studies suggesting that increasing the crosslinker content could lead to higher surface areas,[10,27] the opposite trend was obtained in this study, see Fig. 4E (and Fig. S8B for the N_2 isotherms). When the crosslinker content was increased, with crosslinker/precursor molar ratios ranging from 0.5 to 2, the A_{BET} did not change significantly; it decreased by approximately 50 $m^2\ g^{-1}$, while the reaction yield decreased from 94 to 61 wt%, see Fig. 4E. However, for crosslinker/precursor molar ratios of 0.1 and 0.25, the A_{BET} dropped dramatically to 70–75 $m^2\ g^{-1}$. In the absence of crosslinker, the A_{BET} decreased further to 39 $m^2\ g^{-1}$, accompanied by a decrease in reaction yield to 80 wt%. For comparison, a test was conducted using a lower catalyst and crosslinker content, *i.e.*, a precursor/catalyst/crosslinker molar ratio of 1/2/1. The A_{BET} then decreased to 94 $m^2\ g^{-1}$ compared with the 385 $m^2\ g^{-1}$ obtained for the 1/2/2 sample. The loss of area observed for samples 1/6/[0–2] compared with samples 1/2/[1–2] might be attributed to the higher catalyst content, which facilitates the simultaneous onset of SC and FC reactions. Conversely, the lower catalyst content reduces the likelihood of both reactions occurring simultaneously, ultimately resulting in HCPs with lower A_{BET}.

3.5 Deplete naphthalene oil (DNO)-derived HCPs

The effect of reaction time in DNO-derived HCPs was studied using a precursor/catalyst/crosslinker molar ratio of 1/2/2. Subsequently, in parallel with the study of creosote-derived HCPs, the effect of crosslinker content was assessed while maintaining a constant amount of catalyst, *i.e.*, using precursor/catalyst/crosslinker molar ratios 1/6/[0–2].

3.5.1 Effect of reaction time. The FTIR spectra of DNO-derived HCPs were similar to those observed for creosote-derived HCPs, see Fig. S10. Consequently, at a fixed 1/2/2 molar ratio, a reaction time of 15 min appeared to be optimal for generating more intense signals around 1694 and 1602 cm^{-1} compared to the peak at 753 cm^{-1}, see Fig. S10A, confirming the reduction of C–H units and increase in –C=C– units, which inherently contribute to the formation of the hypercrosslinked structure. Prolonged reaction times may potentially compromise the structure already formed, thereby explaining the reduced intensity of peaks associated with the presence of –C=C– units.

TGA of the DNO-derived HCPs is reported in Fig. 5A, S11 and Table S16. Generally, for DNO-derived HCPs obtained using different reaction times and a 1/2/2 molar ratio, the TG curves followed similar paths up to ~300 °C, showing a small thermal

Open Access Article. Published on 28 April 2026. Downloaded on 6/2/2026 10:49:01 AM.
This article is licensed under a Creative Commons Attribution-NonCommercial 3.0 Unported Licence.

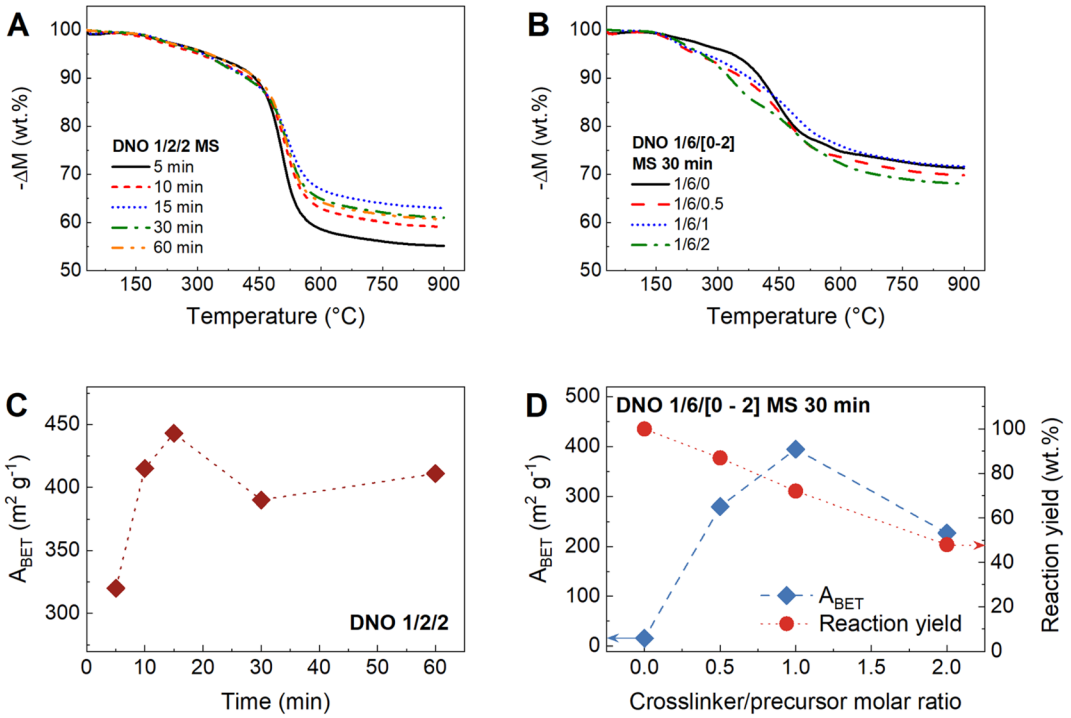

Fig. 5 TG analysis mass loss curves of DNO-derived HCPs obtained by MS: (A) after different reaction times and (B) using different crosslinker contents (1/6/[0–2] molar ratio) and a fixed reaction time of 30 min. (C) A_{BET} for DNO-derived HCPs after MS at different reaction times. (D) A_{BET} and reaction yields of DNO-derived HCPs obtained by MS using different crosslinker contents (1/6/[0–2] molar ratio) and a fixed reaction time of 30 min.

event at ~215 °C. For reaction times of 15 min and longer, the curves showed the emergence of a second small thermal event at ~350 °C, see Fig. S11 and 5A. Variations in degradation rate became more significant during the third thermal event at ~510 °C, see Fig. S11C. It appears that 15 min was the optimal reaction time for achieving high thermal stability, as it had the highest R_{900} in the series, 63 wt% (inset in Fig. S11C). Moreover, the MaSp results also evidenced some differences between the HCPs. Firstly, methane loss increased with reaction time, as shown in Fig. S12A, while no significant difference was observed for the methoxy units. As for toluene, a longer reaction time was associated with a greater release of this compound, see Fig. S12B. However, benzene release was shown to be the lowest for the HCP obtained after a reaction time of 15 min, which explains its higher R_{900} after TG analysis. This trend was unexpected as it contradicts the behavior observed in creosote-derived HCPs, highlighting the importance of the precursor on the stability and final properties of the resulting material. The A_{BET} calculated from the N_2 isotherms are shown in Fig. 5C, indicating an optimum reaction time of 15 min to obtain the highest area, 445 $m^2\ g^{-1}$. Nevertheless, comparable values were obtained within the 10–60 min range, and the A_{BET} consistently exceeded 400 $m^2\ g^{-1}$ for almost all the tested reaction times, suggesting that DNO is more suitable than creosote for the formation of porous HCPs.

3.5.2 Effect of crosslinker content. The effect of crosslinker content was studied using 1/6/[0–2] samples by FTIR analysis, see Fig. S10B. First, for molar ratios 1/6/0 and 1/6/1, high intensities of peaks centered around 1444, 875, 822, 759 and 730 cm^{-1} were detected. Conversely, the peak at 1689 cm^{-1} exhibited its maximum intensity in the 1/6/2 sample. The signals around 1680 and 1440 cm^{-1} were attributed to a better crosslinked structure. This suggests that FC and SC reactions, promoted by higher and lower crosslinker content, respectively, produced bonds whose signatures appear at different wavenumbers. Furthermore, in the case of the 1/6/0.5 ratio, a decrease in the intensity of the 694 cm^{-1} peak was observed. This peak is typically linked to a higher degree of crosslinking, concomitant with an increase in the intensity of the signals at 1694 and 1440 cm^{-1}. However, this pattern was not observed in the 1/6/0.5 sample. Consequently, it is possible that this particular amount of crosslinker resulted in an intermediate state that hampered the formation of the polymer structure.

TGA of DNO-derived HCPs with different crosslinker contents revealed a distinct trend compared to creosote-derived HCPs, see Fig. S11B and D. Notably, the 1/6/1 ratio exhibited the highest R_{900} at 72 wt%, whereas similar values were obtained for the 1/6/0.5 and 1/6/0 molar ratios, 70 and 71 wt%, respectively (see inset in Fig. S11D). However, closer examination of the thermal events revealed significant differences. The mass loss during the first thermal event, at around 200 °C, increased with crosslinker content. Three additional thermal events were observed in the case of the 1/6/0 ratio, with the greatest loss of mass occurring at ~370 °C, 21 wt%. Conversely, a single thermal event was evident for the 1/6/0.5 ratio at temperatures above ~250 °C, resulting in a mass loss of 25 wt%. Indeed, the

© 2026 The Author(s). Published by the Royal Society of Chemistry

Open Access Article. Published on 28 April 2026. Downloaded on 6/2/2026 10:49:01 AM.
This article is licensed under a Creative Commons Attribution-NonCommercial 3.0 Unported Licence.

occurrence of several thermal events is observed for higher crosslinker contents, generally occurring at lower temperatures than those encountered in the case of the HCP obtained with the 1/6/0.5 ratio, see Table S16 for additional details.

The trend observed in the release of methane and methoxy units mirrors that of creosote-derived HCPs, *i.e.*, it decreased with decreasing crosslinking content, see Fig. S12C. This phenomenon is due to the increased prevalence of the crosslinker, resulting in a higher concentration of methylene and non-crosslinked moieties within the structure. Subsequently, these moieties were released in the form of methane and methoxy units, respectively. Similarly, benzene and toluene units were also released in higher concentrations from HCPs with higher relative FDA contents, see Fig. S12D. MaSp analysis from 10 to 300 *m*/*z* revealed another similarity with creosote-derived HCPs. Once again, the samples with low catalyst contents released high-weight molecules, such as 115, 128, 141, 142 and 156 *m*/*z* (data not shown). These units also appeared when analyzing creosote-derived HCPs.

The A_{BET} of DNO-derived HCPs is shown in Fig. 5D. An optimum condition for achieving the highest A_{BET} was identified at a crosslinker/precursor molar ratio of 1. However, using a precursor/catalyst ratio of 1/6, the A_{BET} did not exceed the threshold of 400 $m^2\ g^{-1}$. Similar to the observations made with creosote-derived HCPs, higher reaction yields were achieved by reducing the crosslinker content, potentially reaching 100 wt%. However, eliminating FDA from the formulation significantly reduced the A_{BET}, which fell to 15 $m^2\ g^{-1}$. Thus, although the SC reaction using the 1/6/0 molar ratio is capable of generating an HCP with a strong structure, as suggested by the TG/MaSp results, it does so at the expense of a total loss of porosity.

3.6 Methylene blue adsorption tests

To assess the potential of HCP materials for wastewater remediation, the adsorption of methylene blue (MB), serving as a model compound, was conducted. The results for the HCPs tested are shown in Fig. 6A and detailed in Table S17. Creosote-derived HCPs synthesized with various catalyst contents after a 5-minutes reaction time were evaluated. As observed, relatively low adsorption capacities were achieved, the highest MB adsorption value being 36 $mg_{MB}\ g_s^{-1}$ for the creosote-derived HCP synthesized using the 1/4/2 molar ratio. However, when analyzing samples with the highest A_{BET} for both precursors, namely creosote 1/4/2 MS 60 min and DNO 1/2/2 MS 15 min, significantly higher values were obtained. The DNO-derived HCP provided MB adsorption values of around 87 $mg_{MB}\ g_s^{-1}$ while the creosote-derived HCP achieved MB adsorption values of 102 $mg_{MB}\ g_s^{-1}$. A comparison with the performance of other HCPs reported in the literature is also presented in Fig. 6A.[30–39]

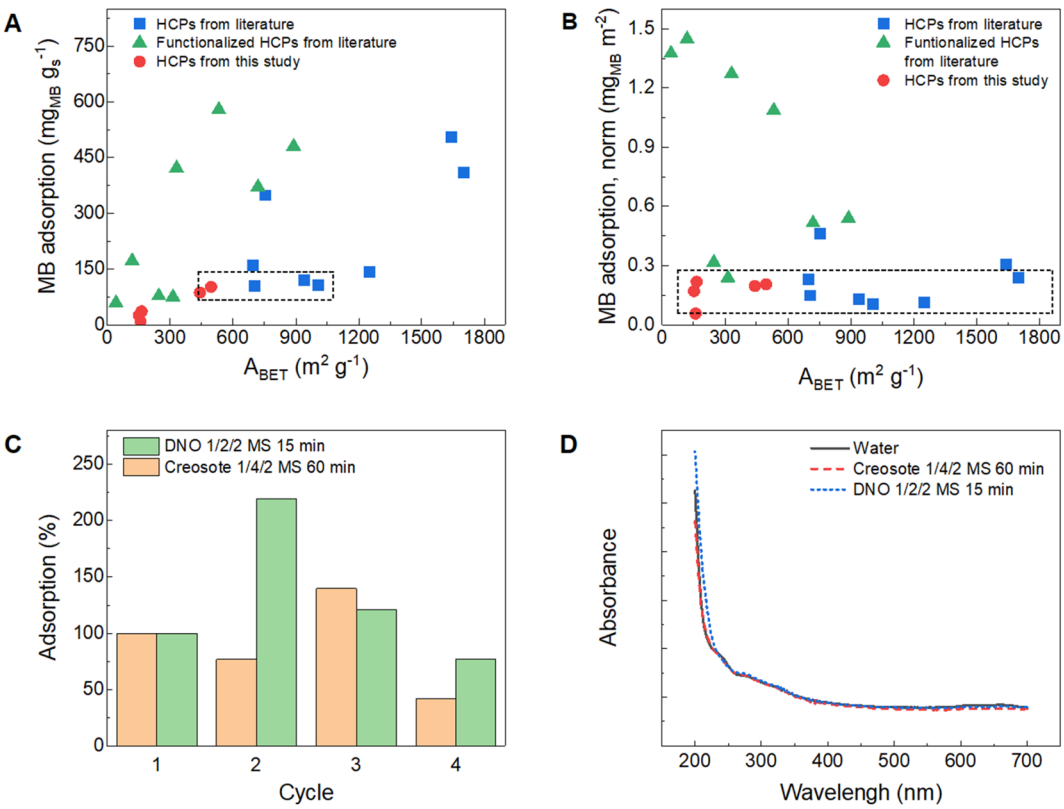

Fig. 6 (A) MB adsorption capacity and (B) normalized (by A_{BET}) MB adsorption capacity as a function of A_{BET} of HCPs from this study compared with that of other HCPs and functionalized HCPs found in the literature.[30–39] (C) Reuse results and (D) UV-vis analysis of water suspensions of creosote- and DNO-derived HCPs with the highest A_{BET} and best MB adsorption performance, namely creosote 1/4/2 MS 60 min and DNO 1/2/2 MS 15 min.

© 2026 The Author(s). Published by the Royal Society of Chemistry

Open Access Article. Published on 28 April 2026. Downloaded on 6/2/2026 10:49:01 AM. This article is licensed under a Creative Commons Attribution-NonCommercial 3.0 Unported Licence.

As expected, MB adsorption capacity generally increases with A_{BET}, a behavior also observed for functionalized HCPs. However, it is important to note that the performance of the best creosote-derived HCP is comparable, for instance, to that of the *p*-dichloroxylene- and benzene (BE-XDC)-derived HCP obtained by Zhao *et al.*,[30] who reported an MB adsorption capacity of up to 105 $mg_{MB}\ g_s^{-1}$, or that of an HCP obtained from Styrofoam waste as a precursor by Dong *et al.*,[31] with a maximum adsorption capacity of 106 $mg_{MB}\ g_s^{-1}$. Shen *et al.*[32] synthesized an anionic HCP from sodium tetraphenylboron (STPB) that exhibited a maximum adsorption capacity of 120 $mg_{MB}\ g_s^{-1}$. It should be noted that, in these cases, the A_{BET} of the HCPs was higher, measuring 706, 939, and 1007 $m^2\ g^{-1}$ for the HCPs derived from BE-XDC, STPB and Styrofoam, respectively (see the dotted rectangle in Fig. 6A). These results, when compared with those reported herein, suggest a greater affinity of the creosote-derived HCP structure for MB than the structures generated in those studies. Indeed, when comparing the MB adsorption capacity normalized by the A_{BET} of the materials, shown in Fig. 6B, it becomes clear that the performance of all non-functionalized HCPs remains between 0.11 and 0.24 $mg_{MB}\ m^{-2}$, regardless of A_{BET}. Conversely, larger differences are found for the performance of functionalized HCPs,[35–39] highlighting the effect of modified surface chemistry in enhancing the materials' affinity for MB molecules. Therefore, in order to enhance the performance of HCPs as adsorbents, it is imperative to optimize the synthesis process or explore other techniques, such as carbonization and/or activation or doping, to further develop their textural properties and/or affinity toward MB.

Besides, the efficiency of HCPs in several adsorption/desorption cycles was tested to analyze the reusability of these adsorbents. Fig. 6C shows the unexpected results obtained. In the second cycle for DNO 1/2/2 MS 15 min and in the third for creosote 1/4/2 MS 60 min, the samples did not lose efficiency; on the contrary, they demonstrated higher MB removal capacities than the HCP used during the first cycle. This phenomenon could be attributed to two potential factors: (i) a certain occlusion of the pores that had been opened by successive ethanol washes or (ii) pore opening due to the elastic nature of HCPs. In general, MB removal performance was better maintained by the DNO-derived sample than by the creosote-derived sample, as evidenced by the final values observed in the fourth cycle.

Finally, to assess the stability of the HCPs and check whether they might release contaminants into the remediated waters they are intended to treat, these samples were put in contact with clean water and analyzed after being stirred for 4 days at 50 °C. As shown in Fig. 6D, UV-vis spectra revealed no evidence that either creosote- or DNO-derived HCPs had released compounds into the aqueous environment.

4 Conclusions

This study highlights the potential of using hazardous coal tar products (CTPs) to synthesize hyper crosslinked polymers (HCPs) by a solvent-free mechanosynthesis method. By exploring various synthesis conditions, we observed a significant impact on the degree of crosslinking of the HCPs obtained, directly influencing their yields. Notably, we found that reducing the crosslinker content led to higher reaction yields, underscoring the critical role of synthesis conditions. Moreover, while the BET area (A_{BET}) of CTP-derived HCPs was slightly lower than that derived from pure benzene, notable A_{BET} values approaching 500 $m^2\ g^{-1}$ were achieved under optimized conditions. Importantly, our HCPs exhibited good adsorption capacities for methylene blue (MB) with respect to their moderate A_{BET}, reaching 10.2 *g* MB per 100 *g* of HPC. Equally significant is the observed stability of these materials in water, even under prolonged immersion and at moderate temperatures, which bodes well for their practical application in wastewater treatment.

In terms of practical implications, our study not only offers a new avenue for transforming hazardous industrial by-products into value-added materials but also highlights the feasibility of employing mechanosynthesis to produce HCPs from a variety of precursors. For instance, the synthesis protocol presented herein could serve as a basis for the more sustainable production of new HCPs derived from other by-products, such as wood tars.

This not only addresses environmental concerns by valorizing waste, but also aligns with the objective of Responsible Production set out in the UN's Sustainable Development Goals. Looking ahead, further optimization of synthesis conditions and exploration of complementary techniques could enhance the porosity and surface chemistry of HCPs, thereby unlocking their full potential as adsorbents for wastewater treatment. This research represents a significant step towards greener and more sustainable materials synthesis practices, paving the way for future advances in wastewater treatment technologies.

Conflicts of interest

There are no conflicts to declare.

Data availability

The data supporting this article have been included as part of the supporting information (SI). Supplementary information is available. See DOI: https://doi.org/10.1039/d5mr00101c.

Acknowledgements

We acknowledge Bilbaina de Alquitranes S. A. (Lutxana-Barakaldo, Spain) and the research group "Carbon Materials" at INCAR-CSIC (Oviedo, Spain) for their invaluable assistance in conducting the chemical composition analysis of the coal tar products. Bernard Noppen (UHasselt) is acknowledged for the TD-GC-MS measurements. This work was funded by the European Union (EU), Research Fund for Coal and Steel (RFCS), through the project UCGWATER + under Grant Agreement No. 101033964 and by the European Regional Development Fund (ERDF) projects TALiSMAN and TALiSMAN 2. A. M. B.-L. also thanks the Margarita Salas grant (SOL-RPU-59) received.

 © 2026 The Author(s). Published by the Royal Society of Chemistry

Open Access Article. Published on 28 April 2026. Downloaded on 6/2/2026 10:49:01 AM. This article is licensed under a Creative Commons Attribution-NonCommercial 3.0 Unported Licence.

References

1 B. Li, X. Yang, L. Xia, M. I. Majeed and B. Tan, Hollow Microporous Organic Capsules, *Sci. Rep.*, 2013, **3**(1), 2128, DOI: 10.1038/srep02128.

2 Y. Gu, S. U. Son, T. Li and B. Tan, Low-Cost Hypercrosslinked Polymers by Direct Knitting Strategy for Catalytic Applications, *Adv. Funct. Mater.*, 2021, **1**, 2008265, DOI: 10.1002/adfm.202008265.

3 J. Du, H. Ouyang and B. Tan, Porous Organic Polymers for Catalytic Conversion of Carbon Dioxide, *Chem.–Asian J.*, 2021, **16**, 1–19, DOI: 10.1002/asia.202100991.

4 A. Waheed, N. Baig, N. Ullah and W. Falath, Removal of Hazardous Dyes, Toxic Metal Ions and Organic Pollutants from Wastewater by Using Porous Hyper-Cross-Linked Polymeric Materials: A Review of Recent Advances, *J. Environ. Manage.*, 2021, **287**, 112360, DOI: 10.1016/j.jenvman.2021.112360.

5 H. Masoumi, A. Ghaemi and H. G. Gilani, Evaluation of Hyper-Cross-Linked Polymers Performances in the Removal of Hazardous Heavy Metal Ions: A Review, *Sep. Purif. Technol.*, 2021, **260**, 118221, DOI: 10.1016/j.seppur.2020.118221.

6 V. E. Shiryaeva, T. P. Popova, A. A. Korolev, A. Y. Kanat'eva and A. A. Kurganov, Stationary Phase Based on Hypercrosslinked Polystyrene for Capillary Gas Chromatography, *Russ. J. Phys. Chem. A*, 2020, **94**(9), 1930–1935, DOI: 10.1134/S0036024420090253.

7 P. Ramirez-Vidal, F. Suárez-García, R. L. S. Canevesi, A. Castro-Muñiz, P. Gadonneix, J. I. Paredes, A. Celzard and V. Fierro, Irreversible Deformation of Hyper-Crosslinked Polymers after Hydrogen Adsorption, *J. Colloid Interface Sci.*, 2022, **605**, 513–527, DOI: 10.1016/j.jcis.2021.07.104.

8 J. Huang and S. R. Turner, Hypercrosslinked Polymers: A Review, *Polym. Rev.*, 2018, 1–41, DOI: 10.1080/15583724.2017.1344703.

9 A. M. Borrero-López, A. Celzard and V. Fierro, Eco-Friendly Production of Hyper-Cross-Linked Polymers Using Mechanosynthesis and Bioresources: A Critical Review, *ACS Sustainable Chem. Eng.*, 2022, **10**(49), 16090–16112, DOI: 10.1021/acssuschemeng.2c04954.

10 J. S. M. Lee, T. Kurihara and S. Horike, Five-Minute Mechanosynthesis of Hypercrosslinked Microporous Polymers, *Chem. Mater.*, 2020, **32**(18), 7694–7702, DOI: 10.1021/acs.chemmater.0c01726.

11 B. Pei, X. Xiang, T. Liu, D. Li, C. Zhao, R. Qiu, X. Chen, J. Lin and X. Luo, Preparation of Chloromethylated Pitch–Based Hyper–Crosslinked Polymers and an Immobilized Acidic Ionic Liquid as a Catalyst for the Synthesis of Biodiesel, *Catalysts*, 2019, **9**(11), 963, DOI: 10.3390/catal9110963.

12 N. Liu, J. Chen, Z. Wu, P. Zhan, L. Zhang, Q. Wei, F. Wang and L. Shao, Construction of Microporous Lignin-Based Hypercross-Linked Polymers with High Surface Areas for Enhanced Iodine Capture, *ACS Appl. Polym. Mater.*, 2021, **3**(4), 2178–2188, DOI: 10.1021/acsapm.1c00139.

13 S. Grätz, S. Zink, H. Kraffczyk, M. Rose and L. Borchardt, Mechanochemical Synthesis of Hyper-Crosslinked Polymers: Influences on Their Pore Structure and Adsorption Behaviour for Organic Vapors, *Beilstein J. Org. Chem.*, 2019, **15**, 1154–1161, DOI: 10.3762/bjoc.15.112.

14 H. Gao, L. Ding, H. Bai, A. Liu, S. Li and L. Li, Pitch-Based Hyper-Cross-Linked Polymers with High Performance for Gas Adsorption, *J. Mater. Chem. A*, 2016, **4**(42), 16490–16498, DOI: 10.1039/c6ta07033g.

15 L. Jia, B. Niu and J. Jiao, Parameter Effects on Dynamic Adsorption of Trichloroethylene on Hypercrosslinked Polymeric Adsorbents, *J. Environ. Eng.*, 2020, **146**(8), 04020082, DOI: 10.1061/(asce)ee.1943-7870.0001759.

16 Z. Wu, W. Wei, J. Ma, J. Luo, Y. Zhou, Z. Zhou and S. Liu, Adsorption of Iodine on Adamantane-Based Covalent Organic Frameworks, *ChemistrySelect*, 2021, **6**(38), 10141–10148, DOI: 10.1002/slct.202102656.

17 R. Castaldo, G. Gentile, M. Avella, C. Carfagna and V. Ambrogi, Microporous Hyper-Crosslinked Polystyrenes and Nanocomposites with High Adsorption Properties: A Review, *Polymers*, 2017, **9**(12), 651, DOI: 10.3390/polym9120651.

18 M. Guerritore, R. Castaldo, B. Silvestri, R. Avolio, M. Cocca, M. E. Errico, M. Avella, G. Gentile and V. Ambrogi, Hyper-Crosslinked Polymer Nanocomposites Containing Mesoporous Silica Nanoparticles with Enhanced Adsorption towards Polar Dyes, *Polymers*, 2020, **12**(6), 1388, DOI: 10.3390/polym12061388.

19 R. Vinodh, P. Hemalatha, M. Ganesh, M. M. Peng, A. Abidov, M. Palanichamy, W. S. Cha and H. T. Jang, Novel Microporous Hypercross-Linked Conjugated Quinonoid Chromophores with Broad Light Absorption and CO2 Sorption Characteristics, *RSC Adv.*, 2014, **4**(8), 3668–3674, DOI: 10.1039/c3ra45466e.

20 Y. Hirabayashi, N. Kato, M. Mizuta and H. Ishihara, *The 3020 cm^{-1} Band in the Infrared Absorption Spectra of Methyl Esters of Unsaturated Higher Fatty Acids*, Bulletion of the Chemical Society of Japan, 1971, vol. 44, pp. 2733–2736.

21 R. Vinodh, A. Abidov, M. M. Peng, C. M. Babu, M. Palanichamy, W. S. Cha and H. T. Jang, A New Strategy to Synthesize Hypercross-Linked Conjugated Polystyrene and Its Application towards CO2 Sorption, *Fibers Polym.*, 2015, **16**(7), 1458–1467, DOI: 10.1007/s12221-015-5151-y.

22 F. Begni, E. Lasseuguette, G. Paul, C. Bisio, L. Marchese, G. Gatti and M. C. Ferrari, Hyper Cross-Linked Polymers as Additives for Preventing Aging of Pim-1 Membranes, *Membranes*, 2021, **11**(7), 463, DOI: 10.3390/membranes11070463.

23 Z. Liu, H. Liu, Y. Wang, H. Yu and J. Wang, *Preparation of Hypercrosslinked Polymers with Cashew Nut Shell Liquid for Removal of Volatile Organic Compounds*, 2022, pp. 1823–1832, DOI: 10.1002/pen.25967.

24 F. Maleki, A. Ghaemi and G. Mir Mohamad Sadeghi, Synthesis and Characterization of Waste Styrofoam Hypercrosslinked Polymer as an Adsorbent for CO_2 Capture, *Environ. Prog. Sustainable Energy*, 2022, **42**(1), e13954, DOI: 10.1002/ep.13954.

Open Access Article. Published on 28 April 2026. Downloaded on 6/2/2026 10:49:01 AM. This article is licensed under a Creative Commons Attribution-NonCommercial 3.0 Unported Licence.

25 S. Grätz and L. Borchardt, Mechanochemical Polymerization-Controlling a Polycondensation Reaction between a Diamine and a Dialdehyde in a Ball Mill, *RSC Adv.*, 2016, **6**(69), 64799–64802, DOI: 10.1039/c6ra15677k.

26 T. Lee, P. T. Dirlam, J. T. Njardarson, R. S. Glass and J. Pyun, Polymerizations with Elemental Sulfur: From Petroleum Refining to Polymeric Materials, *J. Am. Chem. Soc.*, 2022, **144**(1), 5–22, DOI: 10.1021/jacs.1c09329.

27 A. Krusenbaum, J. Geisler, F. Joel, L. Kraus, S. Grätz, M. Valentin, H. Torsten and L. Borchardt, The Mechanochemical Friedel-Crafts Polymerization as a Solvent-Free Cross-Linking Approach toward Microporous Polymers, *J. Polym. Sci.*, 2021, **1**(r), 62–71, DOI: 10.1002/pol.20210606.

28 G. S. Lee, H. W. Lee, H. S. Lee, T. Do, J.-L. Do, J. Lim, G. I. Peterson, T. Friščić and J. G. Kim, Mechanochemical Ring-Opening Metathesis Polymerization: Development, Scope, and Mechano-Exclusive Polymer Synthesis, *Chem. Sci.*, 2022, **13**(39), 11496–11505, DOI: 10.1039/D2SC02536A.

29 A. Krusenbaum, S. Grätz, S. Bimmermann, S. Hutsch and L. Borchardt, The Mechanochemical Scholl Reaction as a Versatile Synthesis Tool for the Solvent-Free Generation of Microporous Polymers, *RSC Adv.*, 2020, **10**(43), 25509–25516, DOI: 10.1039/d0ra05279e.

30 L. Zhao, S. Yuan, J. Sha and S. Li, Hypercrosslinked Polymers Preparation *vs.* Methylene Blue Adsorption, *Mater. Sci. Forum*, 2013, **743–744**, 539–544, DOI: 10.4028/www.scientific.net/MSF.743-744.539.

31 X. Dong, A. Akram, B. Comesaña-Gándara, X. Dong, Q. Ge, K. Wang, S. P. Sun, B. Jin and C. H. Lau, Recycling Plastic Waste for Environmental Remediation in Water Purification and CO_2 Capture, *ACS Appl. Polym. Mater.*, 2020, **2**(7), 2586–2593, DOI: 10.1021/acsapm.0c00224.

32 R. Shen, X. Yan, Y.-J. Guan, W. Zhu, T. Li, X.-G. Liu, Y. Li and Z.-G. Gu, One-Pot Synthesis of a Highly Porous Anionic Hypercrosslinked Polymer for Ultrafast Adsorption of Organic Pollutants, *Polym. Chem.*, 2018, **9**(38), 4724–4732, DOI: 10.1039/C8PY01018H.

33 Y. He, W. Bao, Y. Hua, Z. Guo, X. Fu, B. Na, D. Yuan, C. Peng and H. Liu, Efficient Adsorption of Methyl Orange and Methyl Blue Dyes by a Novel Triptycene-Based Hyper-Crosslinked Porous Polymer, *RSC Adv.*, 2022, **12**(9), 5587–5594, DOI: 10.1039/D1RA08589A.

34 G. Xiong, S. Gao, Q. Zhang, B. Ren, L. You, F. Ding, Y. He and Y. Sun, High Porosity Cyclotriphosphazene-Based Hyper-Crosslinked Polymers as Efficient Cationic Dye MB Adsorbents, *Polymer*, 2022, **247**, 124787, DOI: 10.1016/j.polymer.2022.124787.

35 S. Song, J. Ai, A. Hu, G. Liao and D. Wang, Synthesis of Carboxyl-Modified Hyper-Cross-Linked Polymers with Conspicuous Removal Capability for Various Water-Soluble Contaminants, *J. Environ. Chem. Eng.*, 2021, **9**(5), 106047, DOI: 10.1016/j.jece.2021.106047.

36 F. Li, J. Liu, W. Liu, Y. Xu, Y. Cao, B. Chen and M. Xu, Preparation of Hyper-Cross-Linked Hydroxylated Polystyrene for Adsorptive Removal of Methylene Blue, *RSC Adv.*, 2021, **11**(41), 25551–25560, DOI: 10.1039/D1RA04265C.

37 K. Liu, M. Fu, X. Ma, P. Zhang, S. Zong and W. Zhao, One-Pot Synthesis of Carboxyl-Functionalized Hyper-Cross-Linked Microporous Polymer Based on the Dual-Purpose Reagent Strategy for the Efficient Removal of Methylene Blue from Water, *ACS Appl. Polym. Mater.*, 2023, **5**(12), 9807–9816, DOI: 10.1021/acsapm.3c01529.

38 A. Hu, X. Yang, Q. You, Y. Liu, Q. Wang, G. Liao and D. Wang, Magnetically Hyper-Cross-Linked Polymers with Well-Developed Mesoporous: A Broad-Spectrum and Highly Efficient Adsorbent for Water Purification, *J. Mater. Sci.*, 2019, **54**(3), 2712–2728, DOI: 10.1007/s10853-018-2967-z.

39 J. Wei, J. Jia and T. Liao, Highly Selective Adsorption of Dyes by Functional Hypercrosslinked-Polymers Prepared in a Facile and Chemically Stable Manner, *J. Environ. Chem. Eng.*, 2023, **11**(5), 110555, DOI: 10.1016/j.jece.2023.110555.

 © 2026 The Author(s). Published by the Royal Society of Chemistry